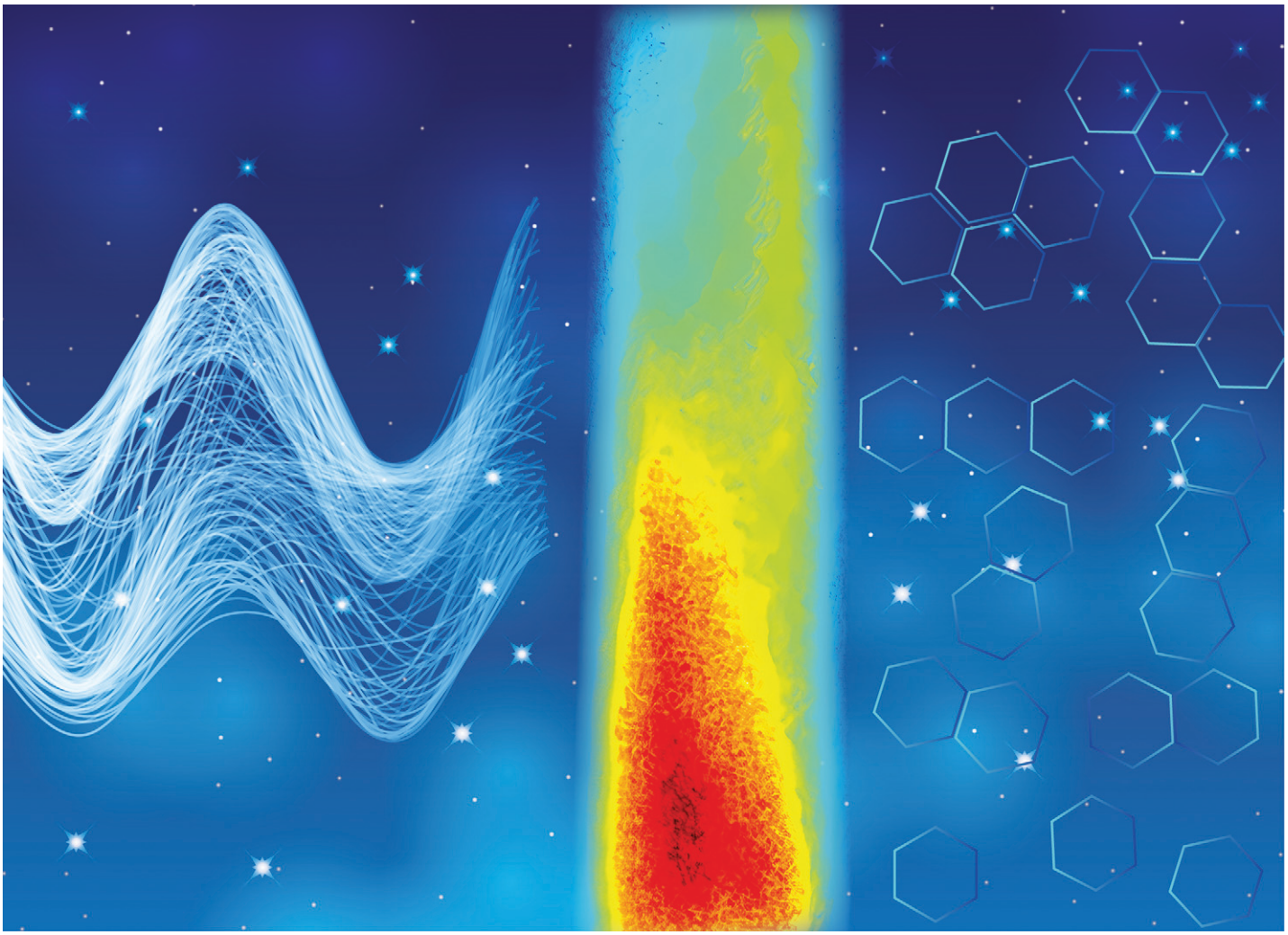

This is a collaborative research between the groups of Professor Ramanarayanan Balachandran, Department of Mechanical Engineering, University College London, and Dr. Roberto Volpe, Department of Chemical Engineering, Queen Mary University of London.

In situ observation of the evolution of polyaromatic tar precursors in packed-bed biomass pyrolysis

In-situ, planar laser-induced fluorescence of vapours from pyrolysing biomass, shows pathways of formation of polyaromatic hydrocarbons in the proximity of the pyrolysing bed.

As featured in:

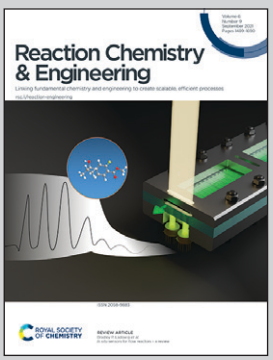

See Roberto Volpe, Midhat Talibi *et al.*, *React. Chem. Eng.*, 2021, **6**, 1538.

ROYAL SOCIETY OF CHEMISTRY

rsc.li/reaction-engineering

Registered charity number: 207890

Reaction Chemistry & Engineering

ROYAL SOCIETY OF CHEMISTRY

PAPER

View Article Online
View Journal | View Issue

Cite this: *React. Chem. Eng.*, 2021, **6**, 1538

In situ observation of the evolution of polyaromatic tar precursors in packed-bed biomass pyrolysis†

Maryanne Chelang'at Mosonik, [a] Roberto Volpe, *[a] Chinonso Ezenwajiaku, [b] Midhat Talibi *[b] and Ramanarayanan Balachandran [b]

Received 24th January 2021,
Accepted 6th May 2021

DOI: 10.1039/d1re00032b

rsc.li/reaction-engineering

Pyrolysis provides a route for the conversion of lignocellulosic biomass into solid, liquid and gaseous energy vectors or platform chemicals. Polycyclic aromatic hydrocarbons (PAHs) generated in the vapour phase of the biomass pyrolytic reaction may condense to form tars, which are difficult to further upgrade and cause process inefficiency. Control of tar production requires optimization of reactor design and careful control of reactor operating conditions. In this study, a vertical resistively-heated fixed-bed reactor is used to study the effect of pyrolysis peak temperatures and holding period (at peak temperature) on the formation of PAHs during pyrolysis of two lignocellulosic biomass samples, walnut shells (WS) and almond shells (AS). '*In situ*' planar laser induced fluorescence (PLIF) is used to optically detect 3-to-5 ring PAHs in the vapour phase immediately above the reactor bed. Results show that the PAH PLIF signal appeared at ~275 °C for the biomass samples and peaked at ~400 °C for WS and ~375 °C for AS, which is in agreement with previous '*off situ*' analysis conducted by the authors. Beyond 400 °C, the PLIF signal was observed to reduce significantly and almost disappear at 550 °C. Initial PAH formation was attributed to condensation reactions occurring due to the drop in temperature along the sample bed. The detection of the PAH PLIF signal itself and its changing intensities, close to the bed, signified the rapid changes the products released from biomass undergo and emphasised the importance of using online techniques for pyrolysis studies. The detailed understanding of the temperature dependent characteristics of PAH formation from this study could help improve reactor design.

1. Introduction

Rising demand for fuels and chemicals produced from sustainable resources, coupled with the push towards low emission energy systems, has propelled research into the utilisation of biomass for clean energy and production of platform chemicals. Pyrolysis is a promising route for the conversion of biomass to useful products. During pyrolysis, biomass is thermally decomposed in the absence of external oxidizing agents, to form solid (char), liquids (bio-oils, tars) and gaseous products.[1] The yield of these three products varies significantly depending on biomass precursors, reactor, sample configuration and process parameters.[2] During slow pyrolysis (~50 K min^{-1} heating rate) in a fixed-bed reactor, carbon content originally present in the untreated feedstock progressively concentrates in the solid phase to form a porous carbonaceous material, known as biochar. The volatiles and ejected liquid products of pyrolysis (bio-oil) are subsequently released from the feedstock[3] and are composed of organic compounds and an aqueous phase.[4] The heavier fraction of the formed bio oils (that is, tar) accounts for up to 70% of the total yield.[5] The amount of tar produced can be controlled through optimization of reactor design and reactor operating conditions, such as peak temperature, pressure, heating rate and residence time.[6] The major components of tar are polycyclic aromatic hydrocarbons (PAHs) and their formation involves bond breaking and cross-linking reactions.[7] PAHs have been identified as a key indicator for tar production during pyrolysis, hence understanding their formation is crucial in order to improve reactor design and operating parameters.[8] However, depending on the desired purpose, tars may be useful for several different applications. Anthracene has been used in the production of anthraquinone dyestuffs (an important class of dyes).[9] Genuino *et al.*[10] recycled the PAH fraction of the pyrolysis of glycerol *via* hydrogenation on a zeolite catalysts in order to improve the yield of benzene, toluene and xylene (BTX).

[a] *School of Engineering and Materials Science, Queen Mary University of London, Mile End Road, London E1 4NS, UK. E-mail: r.volpe@qmul.ac.uk; Tel: +44 (0)20 78827748*
[b] *Department of Mechanical Engineering, University College London, London WC1E 7JE, UK. E-mail: m.talibi@ucl.ac.uk; Tel: +44 (0)20 7694302*

† Electronic supplementary information (ESI) available. See DOI: 10.1039/d1re00032b

Phenanthrene and naphthalene, oxidised to diphenic acid, may be used to manufacture synthetic resins or plasticizers as investigated by Franc.[11] Several research efforts have focused on investigating PAHs generated during biomass pyrolysis. To achieve this, most of these studies have used offline analysis techniques such as gas chromatography coupled to a mass spectrometer (GC-MS), thermogravimetry coupled to MS (TG-MS),[12,13] thermogravimetric balances coupled to Fourier transform infra-red spectroscopy (TGA-FTIR)[14] for the speciation of biomass pyrolysis products. For example, Fabbri *et al.*[8] used GC-MS to detect the 16 priority PAHs (as determined by the US Environmental Protection Agency – EPA) in the liquid pyrolysate of biomass (bio-oil) using two sampling procedures. McGrath *et al.*[15] investigated the effect of change in holding temperatures and gas residence times in the formation of PAHs from cellulose. The authors used GC-MS to identify PAHs and observed that higher temperatures and longer residence times promoted the formation of two, three and four ring PAHs.

However, offline techniques are often affected by different sample collection and preparation conditions such as cooling of the tar or dilution with a solvent, which could introduce errors in their characterisation. This is mainly related to the highly reactive oxygenated compounds present in tars that react during preparation prior to analysis. The more volatile species, such as benzene, volatise while the heavier fraction may polymerise. Furthermore, the presence of reactive compounds cause biomass tars to age faster than the oil derived ones,[16] therefore the time at which tars are analysed after their production influences the analysis outcome. Even when the analyser is placed '*in-line*' during the reaction, it is often installed far from the reaction zone and at different temperature conditions than that of the reaction. Therefore, the products that undergo analysis are not the tars produced during reaction, but rather the tars which have undergone further modifications induced by the method of analysis. This potentially makes virtually all traditional tar analysis biased. In general, the process of tar formation during pyrolysis is an extremely complex and largely unknown process significantly affected by mass and heat transport through a porous solid medium. Tar precursors, formed on the surface of evolving biochars adsorb and desorb from the evolving porous structure of the solid in a similar fashion to what they would do in a chromatographic column.[17] This adsorption–desorption mechanism occurs both at particle and at bed (when present) level. For this reason the biomass sample preparation and configuration and the reactor set-up significantly influence the product outcomes.[2] For all the aforementioned reasons, an accurate analysis of pyrolysis tars requires careful preparation of sample environment and reaction set-up and, ideally, the possibility to observe the evolution pathways of tar formation '*in operando*' in the close proximity of the biomass pyrolysing bed. This is possible using laser induced fluorescence (LIF), a non-intrusive optical diagnostic technique that can provide superior spatio-temporal resolution and does not induce any modification of pyrolysis products during the analysis. Some previous studies have used LIF to study biomass pyrolytic emissions, but only a few have focused on PAHs. Brackmann *et al.*[18] analysed the pyrolysis gases of single birchwood particles and observed fluorescence spectra in the region of 300–500 nm, which was attributed to large hydrocarbons, such 3 and 4 ring aromatics. Zobel *et al.*[19] used LIF to investigate the gaseous reaction products formed from the pyrolysis of large (~25 mm) wood particles. The authors reported an increase in the yields of char and PAHs, which was attributed to an increase in secondary reactions in the heterogeneous vapour–solid phase during pyrolysis. Dieguez-Alonso *et al.*[20] used LIF, optical spectroscopy and (GC-MS) to characterise tar and PAHs from a fixed-bed pyrolyser of pine and beech wood. The results showed that 2 and 3 ring PAHs are released during primary pyrolytic reactions, while longer residence times cause an increase of secondary reactions resulting in the formation of higher fraction of 3 and 4 ring PAHs.

The above review of literature clearly shows the need for capturing the reaction dynamics occurring during tar formation in a biomass bed, especially in instances where there is use of a single biomass particle and the influence of mass transport is disregarded. Hence, our work aims to apply planar laser induced fluorescence (PLIF) to investigate PAH formation in the vapour phase of biomass (WS and AS) pyrolysis just above the reaction zone of a fixed-bed biomass reactor. Planar measurement (PLIF) was preferred over point measurement (LIF) to allow for better spatial and temporal resolution. Experiments were performed to investigate the effect of peak temperature and holding period, while the fluorescence signals emitted from 3-to-5 ring PAHs were captured to provide information on PAHs concentration in the region immediately above the pyrolysing bed and up to 16 mm from it. The results from this study would be particularly useful to unlock potential for use of aromatic compounds from biomass pyrolysis or elimination of these heavier tars. Therefore, regardless of purpose, understanding how, when and where PAHs are formed in the vapour phase of pyrolysing biomass would be useful to 'cherry-pick' desired compounds (or vapours rich in them) as they are formed, to be the building blocks for production of bio-based fuels or chemicals.

2. Methodology

2.1. Fixed-bed reactor setup

A vertical fixed-bed resistively-heated reactor made of a cylindrical stainless steel (SS) tube, 55 cm long and outer diameter (OD) 8 mm, was employed for the pyrolysis. An in-house developed LabVIEW™ software is used to control the power supply and regulate the heating rate. Power is delivered *via* copper clamps which hold the stainless steel tube that serves as a heat exchanger. A feedback loop between a K-type thermocouple and the power supply allows modulation of direct current onto the stainless steel tube that

is therefore resistively heated to finely controlled temperatures and heating rates.

The sample is held in the top 15 mm section of the SS tube held in place between two SS wire mesh. The wire mesh at the top of the bed was 'dome-shaped' to optimize bed packing. Nitrogen (N_2) supplied from the bottom of the SS tube is used to sweep pyrolysis products away while a laser beam intersects the vapors leaving the reaction zone.

A schematic of the experimental setup (including the optical diagnostics, described in the following section) is shown in Fig. 1.

2.2. Optical diagnostics setup

The PLIF setup to detect PAHs has been explained in detail in ref. 21 and briefly described here. PAHs were excited using the 532 nm output from an Nd:YAG laser (Litron Nano PIV) to pump a tunable dye laser containing rhodamine 6G dye. The fundamental wavelength from the dye laser was frequency-doubled and tuned to near 283 nm to give approximately 20 mJ of pulse energy output. In our previous work[21] we reported that the PAH LIF signal is independent of laser intensity variation beyond 8 mJ. In this study we use 20 mJ energy (increased from 12 mJ used in ref. 21) to improve the signal to noise ratio, while the effect of the laser beam profile on the PAH LIF was found to be insignificant at ranges used in the present work. The beam was formed into a light sheet with height and thickness of 50 mm and 0.15 mm respectively using a combination of right-angle prism, plano-concave cylindrical lens (f = −40 mm) and bi-convex lens (f = 500 mm). The sheet was aligned to the central axis of the reactor exit for all measurements.

The fluorescence from the PAH species (from here on referred to as the PAH PLIF signal) was captured with an intensified charge coupled device (ICCD) camera fitted with an f/1.2 Nikon lens of focal length 50 mm positioned perpendicular to the direction of the laser sheet. A combination of GG420 and BG12 (high and low pass Schott filter) was used with the ICCD to detect PAHs of 3–5 rings between wavelengths 420 nm and 480 nm.[21,22] This range of wave lengths was chosen according to the study of Skoog and co-workers[23] who found that the most intense fluorescent behaviour was found in compounds containing aromatic functional groups with low energy transition levels. In their work they conclude that even though compounds containing aliphatic and alicyclic carbonyl structures or highly conjugated double-bond structures may also exhibit fluorescence, it is insignificant compared to aromatic systems. Accordingly, for pyrolytic tars, PAHs are expected to exhibit the highest fluorescence intensity compared to other non-aromatic compounds present in the vapors.

It should be noted that, as demonstrated by O'Sullivan and Testa[24] the emission spectra of aliphatic ketones does slightly overlap with PAHs, having an emission range between 340 and 540 nm and maxima at 405. However,[25] the absorption cross sectional area of aliphatic ketones is in the order of 10^{-21} cm^2 per molecule compared to PAHs' 10^{-17} cm^2 per molecule. Ultimately, while there might be an overlap of fluorescence between PAHs and aliphatic ketones, this is expected to be negligible owing to 1) a chosen range of wavelength that is beyond the maximum emission for ketones and 2) their cross-sectional area being several orders of magnitude smaller than that of PAHs.

These 100 images were accumulated per condition at a camera frame rate of 10 Hz. The pixel resolution of the detection system within the field of view was 20 μm.

It should be noted that the PAH PLIF signal is considered to be representative of the PAH concentration within the probe volume in this study.

2.3. Sample preparation

Almond shells (AS) and walnut shells (WS) were used as biomass samples in this study, they were sourced from a cultivation field in southern Sicily (Italy). These two biomasses were chosen due to their difference in lignocellulosic content and their relative homogeneity in composition compared to other biomass sources. WS has relatively high lignin (hence high aromatic) content[26] while AS in comparison has lower content, as shown in Table 1.

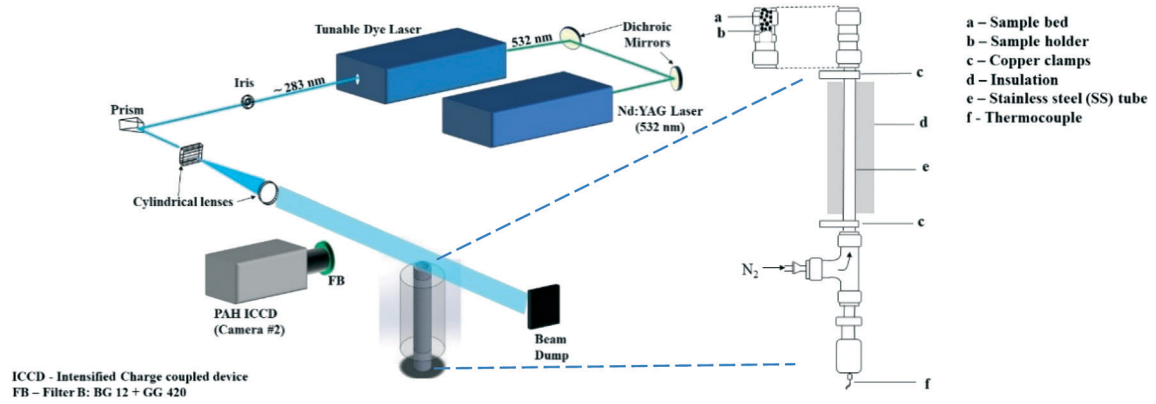

Fig. 1 Schematics of experimental setup and reactor set up.

Table 1 Proximate analyses of AS & WS (wt% dry and ash free)[26]

	Hemicellulose	Cellulose	Lignin	Fixed carbon	Volatile matter	Extractive matter[a]
Walnut shells	22.1	25.6	52.3	37.9	59.3	2.8
Almond shells	28.9	50.7	20.4	22.7	74.0	2.5

[a] Alcohol/benzene (1/1, v/v) extractives.

The samples were milled and sieved to particle sizes of 1–2 mm and oven dried at 105 °C for 48 hours eliminate any moisture. The particles were then stored in a desiccator to ensure samples were kept dry prior to experiments.

2.4. Experimental procedure

A fixed weight of 120 mg was placed in turn for both biomass samples in the reactor and N_2 was flowed through the reactor at a constant flow rate of 2 slpm. The required experimental parameters – holding temperature (HT), heating rate (HR), holding period (HP) – were input in the LabVIEW™ control program. The packed bed sample is about 10 mm tall, this means that the gas residence time in the packed bed will be fast, around <0.001 s. While this calculation does not take into account the volatiles formed during reaction, their low amount compared to the flow of N_2 allows us to safely assume that the temperature of the volatiles escaping the bed is that measured by the thermocouple. HT of 300 °C, 350 °C, 450 °C and 550 °C were used for this investigation. A heating rate of 0.25 °C s^{-1} was used to ramp up to the desired HT. Owing to the slow HR, it is safe to assume that when thermal decomposition takes place at an onset temperature in the proximity of 180–200 °C,[27] any moisture uptake that might have occurred during the handling of the samples prior to experiments would have been eliminated. Images were captured at 25 °C intervals during the heating up stage. Then, when the HT was achieved, the samples were held at that value for 30 minutes, referred to as the HP. Images were also captured at different intervals during the HP. Samples were weighed before and after each run to determine mass loss (char yield, see ESI†). The temperature above the reactor bed was measured at the end of the HP.

2.5. Image analysis

For each case studied, the 100 accumulated images were averaged, and background corrected to minimize any ambient noise effects. An example corrected image of the PAH PLIF signal is shown in Fig. 2a. The PAH PLIF signal can be assumed to be representative of the total PAH concentration in the field of view (or region of interest) The images were analysed using an in-house developed MATLAB® routine. The intensity of the colour in the image correlates with the relative PAH concentration in the volatile phase, with red denoting higher concentration and blue denoting lower concentrations of PAHs.

Reflections from the top of the wire mesh dome at the exit of the reactor were excluded from the image analysis by setting a zero-point 0.4 mm above the dome in the MATLAB® code.

The cumulative PAH signal was determined at different heights (in steps of 20 μm) above the reactor bed up to a height (y) of 16 mm and will be referred to as PAH_{sum}. Fig. 2b shows the PAH_{sum} plotted as a function of height for the image in Fig. 2a.

2.6. Uncertainty and error estimation

The influence of the number of images on the PLIF signal was studied by capturing up to 200 images of the PAH PLIF signal from WS pyrolysis in batches of 50 for the 350 °C holding temperature condition. Averaged images were obtained for different number of images in increasing intervals of 50 (50 images, 100 images and so on) and the variation in the signal value between the averaged images was determined to be within 2%.

The laser energy was kept at 20 mJ per pulse for all the experiments, which ensured that the energy was above the threshold value for PAH fluorescence saturation of 8 mJ per pulse, determined similar to ref. 21. The shot-to-shot variation in laser energy was observed to be within ±10%. Therefore, the PAH_{sum} values can be considered independent of any fluctuation in laser energy.

It should be noted that the shape of the PAH PLIF signal is strongly influenced by the flow pattern resulting from the combined effect of the shape of the wire mesh dome and the 3D geometry of porosity in the heated biomass sample. As the biomass sample is pyrolysed some material loss is expected, which is likely to change the flow configuration above the reactor bed. Some evidence of this was observed in the captured PAH PLIF images, as will be seen in Fig. 2 later.

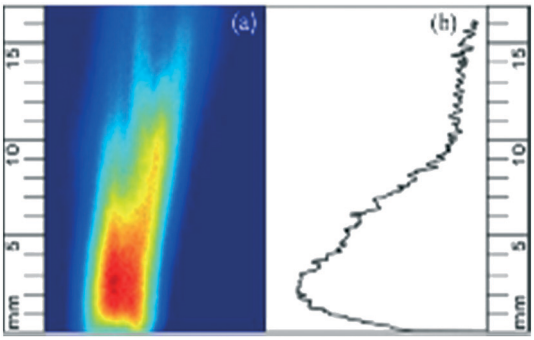

Fig. 2 (a) Background corrected PAH PLIF image and (b) PAH_{sum} profile expressed as a function of height. Red colour denotes higher concentration and blue lower one.

Hence, the cumulative value of PAH signal (PAH_{sum}) has been employed to provide qualitative understanding of PAH formation characteristics and their relative concentration in the volatile mix, using the aforementioned color coding.

3. Results and discussion

Fig. 3 presents the concentration of PAHs.

It is evident from Fig. 3 that, in addition to the changes in PAH PLIF signal, the flow pattern downstream of the dome also changes with increasing temperature. However, for a flow in the laminar regime, it is expected that in close proximity of the dome exit, the effects of buoyancy, flow spread, entrainment on the PAH PLIF signal are insignificant especially in the central axis[28] where the measurements were taken. Hence, analysis for this study will focus on the region, which is in close proximity to the dome, that is up to heights of 10 mm from the dome exit, where changes in the PAH PLIF signal can be considered to be mostly reflective of the pyrolysis process. Fig. 3 shows that the first PAH PLIF signals were observed around 275 °C. These signals could be attributed to one or a combination of the following: (1) 3–5 rings PAHs detaching directly from the bed, (2) 1–2 ring PAHs that have detached from the biomass matrix and coalesced to 3–5 ring structures throughout the bed or in the vapour phase, (3) 3–5 rings aromatics formed in the vapour phase from unsaturated alkenes. It should be noted that the temperature just above the bed is on average ~50 °C lower than the 275 °C measured just under the bed (see section 2.1. for more details). The reduction in temperature through the bed could promote PAH formation in the homogeneous vapour phase as volatiles percolate through the packed bed before escaping it. As hypothesised, these species could be aromatics or also alkenes detached from the solid phase at the bottom of the bed where the temperatures are close to 275 °C. TGA conducted on raw biomass samples by the authors in another study showed that the first DTG peak was detected at 250 °C,[29] which may relate to this sharp increase in signal observed at similar temperature in this study.

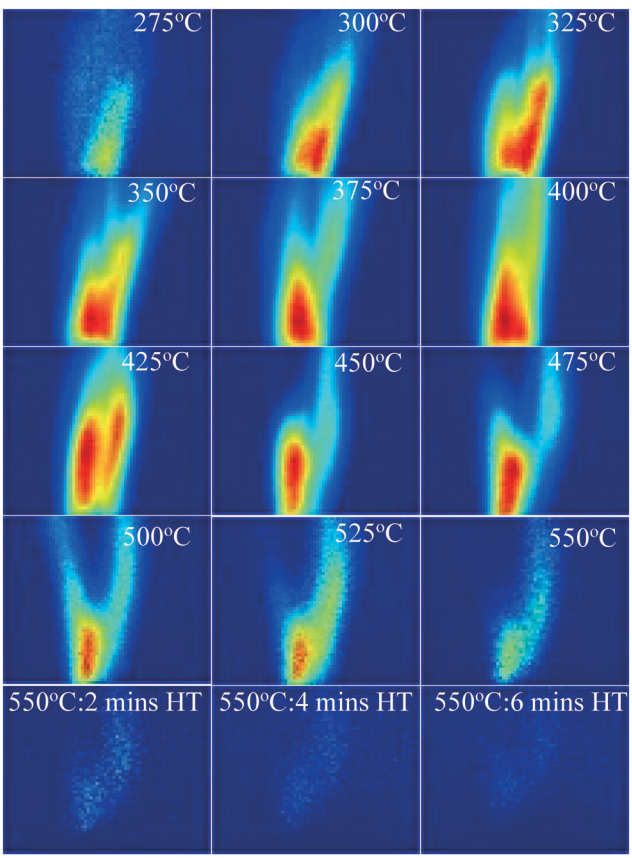

Fig. 3 PAH PLIF images with increasing temperature for the 550 °C HT condition and for maintaining HT for up to 6 minutes for WS. Red colour denotes higher concentration and blue lower one.

As the temperature increases further (Fig. 3), the PAH PLIF signal intensity increases up to about 425 °C before decreasing until the signal completely disappears when the temperature reaches 550 °C and is held at that value for 6 minutes. This increase seems to coincide with the scission of C–H covalent bonds in aliphatic chains that is expected to occur at around 320–330 °C, as was demonstrated in previous studies of similarly packed biomass beds.[30,31] The thermal breakdown of solid particles generates radical fragments that undergo coupling reactions to form aromatic compounds.[29] Fixed-bed reactors are known to promote secondary reactions (such as Diels–Alder) in which biomass particles are stacked on top each other (packed beds). Volatiles moving through the bed react with species both within the particle matrix and on the particle surface in a series of homogeneous (vapour–vapour) or heterogeneous (vapour–solid) reactions.[32] The outer surface of the particles can be expected to be significantly hot as it comes in direct contact with the N_2 sweep gas. Stable free radicals are likely to form on the surface of the solid biomass particles from 300 °C. These radicals are highly reactive and can be expected to react with vapours at those temperatures.[29,33]

The significant reduction in PAHs observed at temperatures above 550 °C could be attributed to one or a combination of the following: (1) the thermal cracking of 3-to-5 ring PAHs into lighter compounds, (2) catalytic cracking of aromatics on hot solid surfaces and (3) condensation/repolymerization of PAHs into a higher number of rings that fluoresce at wavelengths not detected by the imaging equipment (as mentioned earlier, the optical setup employed in this study only allowed detection of 3-to-5 ring PAHs). It should also be noted that the presence of inorganics in the solid matrix during reaction may affect the reactions themselves. This is difficult to calculate in the current set-up, however it is expected to favour the reduction of formation of PAH[34]

The images in Fig. 3 also show that the intensity of the PAH PLIF signal is highest at the central line axis slightly above the pyrolysis reaction zone and reduces with increasing distance away from the high intensity region. This spatial variation in the PAH PLIF signal will be discussed in more detail later.

3.1. Effect of temperature on PAH production

Fig. 4 shows the PAH_{sum} at different heights above the reactor bed during pyrolysis of (a) AS and (b) WS at 25 °C intervals up to 550 °C HT and during 4 minutes of HP. Similar to the trends observed in Fig. 3, it can be seen that PAH_{sum} first increases with increasing temperature before subsequently reducing as the temperature is increased further; this peak occurs between 350 °C and 450 °C in both samples.

These relatively high PAH concentration may also be caused by a set of dehydration reactions occurred at the lower pyrolysis temperatures causing a decrease in the extent of hydrogen bonding and a lowering of the energy required for further decomposition.[30] Beyond 500 °C the rate of cleavage of covalent bond decreases possibly due to sufficient mass loss (see ESI†), reducing the emission of volatiles and hence reducing the PAH signal.

The results in Fig. 4 also show a variation in PAH LIF signal with height above the bed. This is detected for temperatures between 275 and 400 °C. For WS, the PAH LIF signal first increases to peak at about 2.5–3 mm above the reactor bed, and then decreases, while in AS, the signal peaks occur just above the bed and then gradually decrease. Similar trends in the spatial variation of the PAH LIF signal can also be qualitatively observed in Fig. 3. The initial increase in PAH concentration in WS can be attributed to an increase in the rate of 3-to-5 rings PAH formation reactions due to coalescing of smaller rings aromatics in the lower temperature regions above the bed. On the other hand, the reduction in signal can be related primarily to either (1) coalescing of 3-to-5 rings aromatics into heavier compounds (that fall beyond the range of detection) or (2) breaking of 3-to-5 rings PAH into lower number rings compounds (also not within the range of detection). However, the latter seems less plausible due to the lower temperatures in the regions further above the pyrolysing bed.

Fig. 4 clearly shows how the first significant increase in signal occurs at 325 °C for both WS and AS and kept on increasing beyond that temperature up to 400 °C for AS and 425 °C for WS, when signal begins to decay. The PAH_{sum} profiles in Fig. 4 show also an interesting bi-modal type distribution with a second peak 10 mm above the bed for temperatures 325, 350 and 400 °C especially for WS (slightly less pronounced for AS). This means that the concentration of 3-to-5 rings PAHs increases in the vapour phase, most probably due only to homogeneous reactions causing the condensing of lower (<3) rings PAHs into larger compounds as temperature decreases along the area above the packed bed.

3.2. Effect of sample configuration on PAHs

Fig. 5 shows the variation in PAH_{sum} with increasing height above the reactor bed for 300 °C, 350 °C and 450 °C HT. The graphs show the PAH_{sum} profile (1) as the temperature is increased (in 25 °C temperature intervals) up to the holding temperature, and (2) when the HT is maintained for different HP indicated with a subscript in the graph's legends.

Fig. 5 shows how the PAH signal decreases with increasing HP, probably owing to the reduction in the rate of formation of PAHs with time at the same temperature. The figure also shows that as HP increases, the PAH signal decreases more significantly for higher HT. For example, the PAH signal reduced to almost zero when both AS and WS samples are held at 450 °C for 10–15 minutes (Fig. 5c), but significant PAH signal intensity is observed when the samples are maintained at 300 °C even after 30 minutes (Fig. 5a). This observation is also supported by the mass loss during reaction. The solid mass loss at 450 °C was considerably higher at ~70% compared to ~40–50% loss for the 300 °C condition (see ESI†). This is an expected consequence of slower reaction kinetics at lower temperatures. The results presented in Fig. 5 provide useful indications on choice of heating profiles to generate the desired amounts of 3–5 rings aromatics when they could be used as precursors for further upgrade in the synthesis of green chemicals.

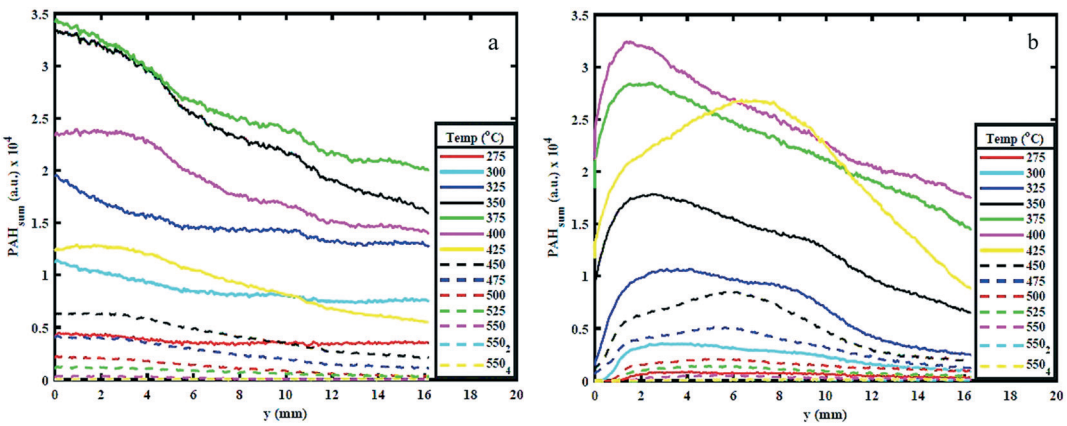

Fig. 4 PAH_{sum} for different temperatures and heights above reactor bed for 550 HT condition for (a) AS and (b) WS.

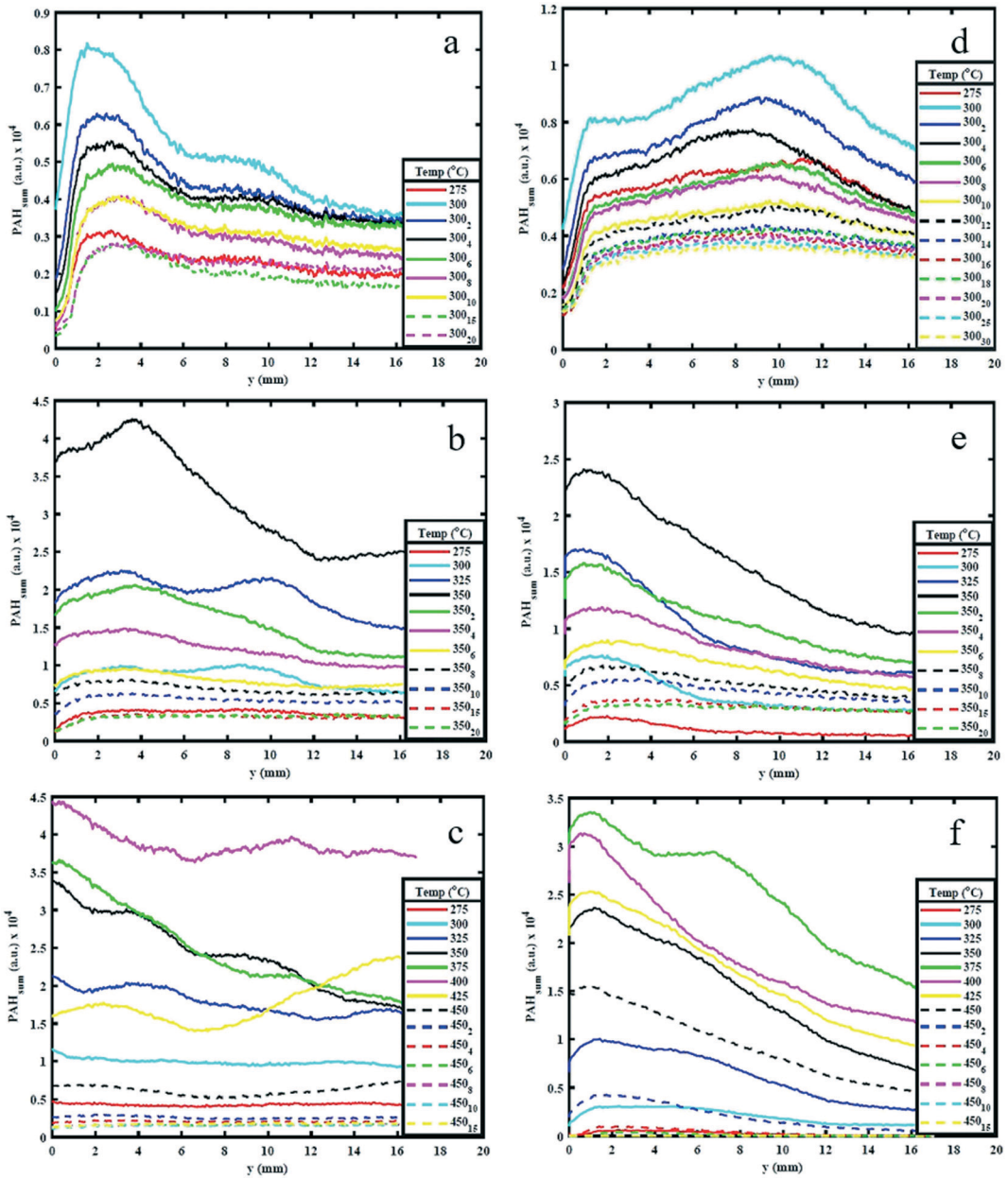

Fig. 5 PAH_{sum} profiles for different holding temperatures for the two biomass samples, AS (a – 300 °C, b – 350 °C and c – 450 °C) and WS (d – 300 °C, e – 350 °C, f – 450 °C). The subscript in the legend indicates the number of minutes the sample is held once the desired holding temperature is reached.

Peak PAH PLIF signal levels are different between AS and WS, as can be seen in Fig. 5. The difference in signal intensity is particularly evident at 350 °C and 450 °C HT, while at 300 °C and 550 °C, this difference is minimal. This can be attributed to the difference in macro-constituents compositions of AS and WS biomass samples. According to Demirbas A.,[26] AS has a higher content of hemicellulose and cellulose than WS, while WS has a higher content of lignin than AS as shown in ref. 26. Different macro-constituents of the ligno-cellulosic matrix contain different bonds and will therefore decompose at different temperatures. The different complexities of the ligno-cellulosic structure are responsible for the variations in the PAH PLIF signal. Cellulose and hemicellulose show relatively simple linear structures; cellulose is a long-chain natural occurring glucose polymer and hemicellulose, while hemicellulose is a heterogeneously branched mixture of polysaccharides.[35] Lignin, on the other hand is a more complex three dimensional amorphous cross-linked polymers arising from oxidative coupling of three primary precursors, *ρ*-coumaryl, coniferyl and sinapyl alcohols.[36] Owing to these differences in structure, the decomposition of ligno-cellulosic macro constituents occurs at different temperatures and reaction times. Though the macro-constituents may act synergistically during

decomposition of biomass,[37,38] the thermal degradation of hemicellulose and cellulose generally occurs (or starts to occur) at relatively lower temperatures between 220 °C and 400 °C and progresses relatively fast, while lignin decomposition is more complex and occurs more slowly over a wide temperature range between 160 °C to 900 °C.[39] Comparing the hemicellulose, and cellulose content in both samples as shown in Table 1, one can observe that this content is higher in AS than it is WS. Accordingly, at 275 °C and 300 °C, AS initial decomposition rate is higher than WS.

3.3. Effect of holding temperature on PAHs

Fig. 6(a) and (c) shows the effect of HT on the maximum PAH concentration (referred to as PAH_{max}), while Fig. 6(b) and (d) shows the effect of HP on PAH_{max}. The value of PAH_{max} is the highest value of PAH_{sum} obtained from profiles determined from Fig. 4 and 5 for the different HTs. It can be seen from Fig. 6(a) that highest value of PAH_{max} occurs around 400 °C for WS and 350 °C for AS and the rate of increase of PAH_{max} with temperature is linear while the rate of decay of PAH_{max} (only apparent for the 550 °C holding temperature condition) is non-linear. The peak PAH signal temperature of 400 °C and 350 °C is in-line with the observations made earlier from the PAH PLIF images and PAH_{sum} profiles, while the increase in PAH PLIF signal can be coupled to the occurrence of free radicals on the surface of solid biomass particles and cleavage of covalent bonds between 300–500 °C, as explained earlier. It should be noted that for the 450 °C and 550 °C HT condition, the reduction in PAH_{max} occurs when the temperature is still being increased up to the holding temperature and continues to decrease as the respective HT is maintained, while for the 300 °C and 350 °C HT condition the PAH_{max} decay starts after the HT is reached, as can be observed from Fig. 6(b) and (d). This is as expected since higher temperatures induce faster kinetics, higher rate of release of volatiles and hence higher rate of formation of PAHs. However, it seems that the PAH formation peaks when the biomass sample reaches temperatures of about 375–400 °C for WS and 325–375 °C for AS irrespective of the HT. This difference may again be related to the higher lignin content in WS. As observed,

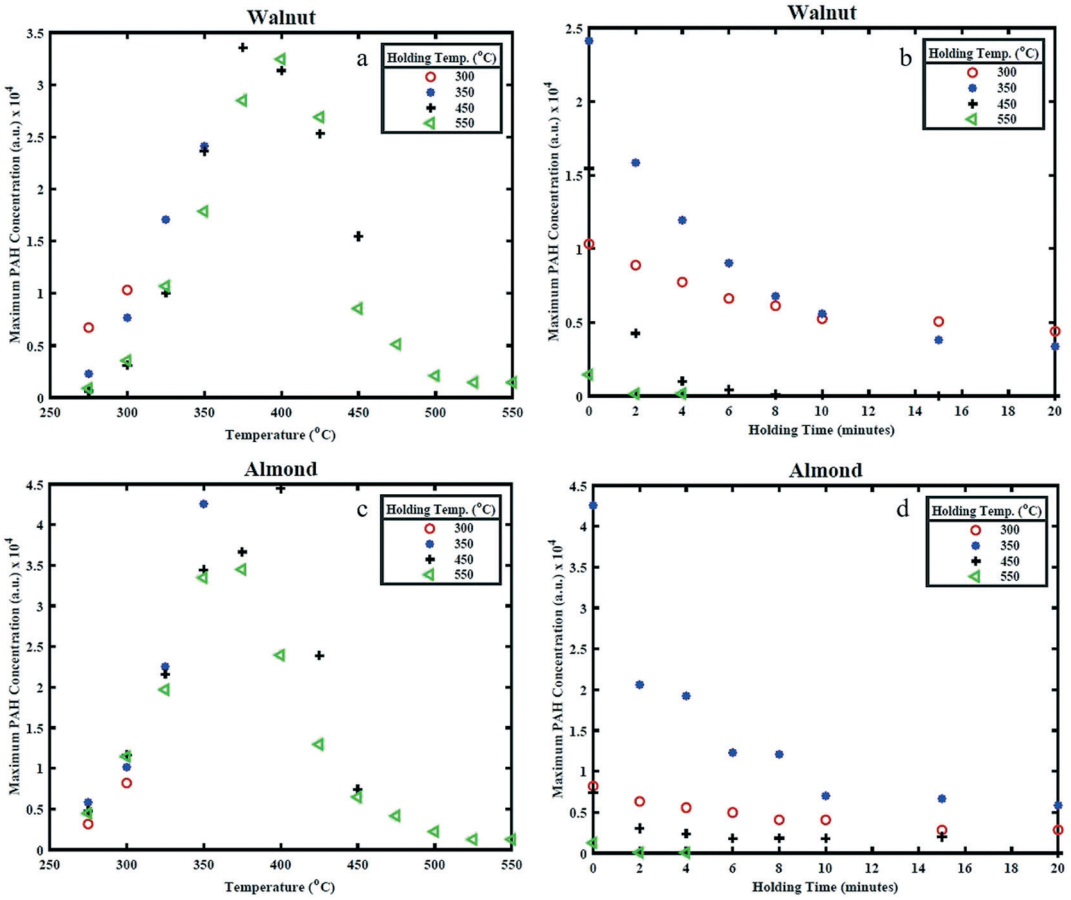

Fig. 6 Maximum PAH concentration (representing maximum PAH LIF signal) for different (a) and (c) holding temperatures and (b) and (d) holding period.

increasing the temperatures higher than those values leads to a reduction in the PAH concentration. This is related to an expected reduction in the release rate of volatile species beyond 350 °C as discussed.

Between 350 and 450 °C, the PAH LIF intensity is higher in WS than in AS. This again could be attributed to the higher lignin content (higher energy bonds) in WS than AS. In Fig. 6, the PAHs concentrations levels from AS increase with temperature to reach a maximum at 350 °C and then decrease rather sharply above that temperature. In WS, the PAHs levels increase gradually as HT increase, remain almost non varied at higher temperatures and then decrease more gradually. This may also be related to the higher presence of lignin in WS and hence the more energy needed to decompose it.

4. Conclusions

Detailed experimental investigations were performed to study the effects of pyrolysis peak temperature and HP at peak temperature on the formation of PAHs in the vapour phase during pyrolysis of biomass samples; walnut and almond shells. A vertical resistively-heated fixed bed biomass reactor was utilised for the pyrolysis. Planar laser induced fluorescence (PLIF) technique was employed to optically detect 3-to-5 ring PAHs in the vapour phase of the pyrolysis products just above the reaction zone of the reactor. The following comments below summarise the key conclusions from this study:

- Peak PAH signal was observed about 2.5–3 mm above the reactor bed, which was linked to a reduction in temperatures promoting PAH formation. At higher heights, the PAH PLIF signal decreased possibly due to smaller PAHs fusing to form larger structures which was outside the detection limit of the optical setup. This leads to the conclusion that any change in temperature along the sample collection lines in offline techniques, once the products are released, leads to the rapid change in the released product itself. Therefore, the collected product is entirely different from the released product. This should therefore be taken into account when use of offline techniques is employed.
- PAH PLIF signals were initially observed at temperatures between 250–275 °C close to the reactor for both samples. The detection of the signal was attributed to the coalescing of aromatics and unsaturated alkenes, ejected from the solid particles to form PAHs in the vapour phase.
- PAH PLIF signal was observed to increase up to ~375 °C for AS and ~400 °C for WS before subsequently decreasing, and completely diminishing by 550 °C for both samples. The increase was attributed to cleavage of covalent C–H bonds from aliphatic structures, while the reduction was linked to material loss causing decrease in emission of volatiles. This also meant that this temperature range (350–400 °C) is crucial for pyrolysis, as shown in Fig. 6, as the scission of bonds is maximum at this point.
- The PAH signal reduced to almost zero when both biomass samples were held at 450 °C and 550 °C for 10–15 minutes, but significant PAH signal was observed when the samples were maintained at 300 °C even after 20 minutes. This observation was supported by the percentage loss in mass of the biomass sample – ~40% for the 300 °C HT condition and ~70% for the 450 °C HT condition. Therefore, industrial systems should be modified for their desired purpose, be it production and collection of biofuels gaseous products or char, at the temperatures mentioned above of between 250 °C and 550 °C.
- The differences observed in the results for WS and AS confirms the influence of sample composition on quantity of volatiles produced. Complexity of lignin structure and simplicity of cellulose and hemicellulose structures is the reason for this difference in PAH PLIF signal intensity. Therefore, if a high quantity of volatile production is desired, samples with lower lignin content should be used. Additionally, further spectroscopic analysis could be employed to resolve the various smaller ring PAHs formed during the pyrolysis, which will help to effectively track the growth of PAHs from smaller rings to larger rings.

Nomenclature

HP	Holding period
HT	Holding temperature
PAH	Polycyclic aromatic hydrocarbons
PAH_{sum}	Cumulative of PAH peak profile
PAH_{max}	Maximum of PAH cumulative profile
PLIF	Planar laser induced fluorescence
WS	Walnut shells
AS	Almond shells

Conflicts of interest

There are no conflicts to declare.

Acknowledgements

The authors would like to acknowledge EPSRC (EP/P003036/1) and the Nigerian Petroleum Technology Development Fund (PTDF) for their financial support towards this work.

References

1 Y. Pan and S. Kong, *Combust. Flame*, 2017, **178**, 21–34.
2 M. R. Barr, R. Volpe and R. Kandiyoti, *ACS Sustainable Chem. Eng.*, 2019, **7**(16), 13734–13745.
3 R. Sikkema, H. M. Junginger, W. Pichler, S. Hayes and A. P. C. Faaij, *Biofuels, Bioprod. Biorefin.*, 2010, 132–153.
4 M. Carrier, J. Joubert, S. Danje, T. Hugo, J. Görgens and J. Knoetze, *Bioresour. Technol.*, 2013, **150**, 129–138.
5 M. P. Houben, H. C. De Lange and A. A. Van Steenhoven, *Fuel*, 2005, **84**(7–8), 817–824.
6 C. Di Blasi, *Prog. Energy Combust. Sci.*, 2008, **34**, 47–90.

7 J. Han and H. Kim, *Renewable Sustainable Energy Rev.*, 2008, **12**, 397–416.
8 D. Fabbri, A. Adamiano and C. Torri, *Anal. Bioanal. Chem.*, 2010, **397**, 309–317.
9 H.-G. Franck, J. W. Stadelhofer, H.-G. Franck and J. W. Stadelhofer, in *Industrial Aromatic Chemistry*, Springer, Berlin Heidelberg, 1988, pp. 343–361.
10 H. C. Genuino, I. Muizebelt, A. Heeres, N. J. Schenk, J. G. M. Winkelman and H. J. Heeres, *Green Chem.*, 2019, **21**, 3802–3806.
11 H. G. Franc, *Ind. Eng. Chem.*, 1963, **55**, 38–44.
12 L. Nowicki and S. Ledakowicz, *J. Anal. Appl. Pyrolysis*, 2014, **110**, 220–228.
13 X. Hu, H. Guo, M. Gholizadeh, B. Sattari and Q. Liu, *Biomass Bioenergy*, 2019, **120**, 28–39.
14 X. Yang, Z. Fu, D. Han, Y. Zhao, R. Li and Y. Wu, *Renewable Energy*, 2020, **147**, 1120–1130.
15 T. McGrath, R. Sharma and M. Hajaligol, *Fuel*, 2001, **80**, 1787–1797.
16 R. J. Evans and T. A. Milne, *Chemistry of Tar Formation and Maturation in the Thermochemical Conversion of Biomass*, 1997.
17 T. J. Morgan and R. Kandiyoti, *Chem. Rev.*, 2014, **114**, 1547–1607.
18 C. Brackmann, M. Aldén, P.-E. Bengtsson, K. O. Davidsson and J. B. C. Pettersson, *Appl. Spectrosc.*, 2003, **57**, 216–222.
19 N. Zobel and A. Anca-Couce, *J. Anal. Appl. Pyrolysis*, 2015, **116**, 281–286.
20 A. Dieguez-Alonso, A. Anca-Couce and N. Zobel, *J. Anal. Appl. Pyrolysis*, 2013, **102**, 33–46.
21 C. Ezenwajiaku, M. Talibi, N. A. K. Doan, N. Swaminathan and R. Balachandran, *Int. J. Hydrogen Energy*, 2019, **44**, 7642–7655.
22 L. M. Verhoeven, M. H. de Andrade Oliveira, A. Lantz, B. Li, Z. S. Li, C. C. M. Luijten, J. A. van Oijen, M. Aldén and L. P. H. de Goey, *Proc. Combust. Inst.*, 2013, **34**, 1819–1826.
23 D. Skoog, F. J. Holler and S. R. Crouch, *Principles of instrumental analysis, Cenage Learning*, 7th edn, 2017.
24 M. P. O'Sullivan and A. C. Testa, *J. Am. Chem. Soc.*, 1970, **92**, 5842–5844.
25 H. Keller-Rudek, G. K. Moortgat, R. Sander and R. Sörensen, *Earth Syst. Sci. Data*, 2013, **5**, 365–373.
26 A. Demirbaş, *Energy Sources*, 2002, **24**, 215–221.
27 M. R. Barr, R. Jervis, Y. Zhang, A. J. Bodey, C. Rau, P. R. Shearing, D. J. L. Brett, M.-M. Titirici and R. Volpe, *Sci. Rep.*, 2021, **11**, DOI: 10.1038/s41598-020-80228-x.
28 C. H. C. Chan and K. M. Lam, *Phys. Fluids*, 1998, **10**, 637–644.
29 R. Volpe, J. M. Bermudez Menendez, T. Ramirez Reina, M. Volpe, A. Messineo, M. Millan and M.-M. Titirici, *Fuel*, 2019, **255**, 115802.
30 R. Volpe, A. Messineo and M. Millan, *Fuel*, 2016, **183**, 139–144.
31 R. Volpe, J. M. B. Menendez, T. R. Reina, A. Messineo and M. Millan, *Fuel Process. Technol.*, 2017, **158**, 255–263.
32 M. Gronli, A Theoreical and Experimental Study of Thermal Degradation of Biomass, *PhD Thesis*, The Norwegian University of Science and Technology, 1996.
33 R. Volpe, S. Messineo, M. Volpe and A. Messineo, *Chem. Eng. Trans.*, 2016, **50**, 181–186.
34 M. R. Barr, R. Volpe and R. Kandiyoti, *ACS Sustainable Chem. Eng.*, 2021, **9**, 5603–5612.
35 P. McKendry, *Bioresour. Technol.*, 2002, **83**, 37–46.
36 B. Xiao, X. Sun and R. Sun, *Polym. Degrad. Stab.*, 2001, **74**, 307–319.
37 R. Volpe, A. A. Zabaniotou and V. Skoulou, *Energy Fuels*, 2018, **32**, 8420–8430.
38 A. George, T. J. Morgan and R. Kandiyoti, *Energy Fuels*, 2014, **28**, 6918–6927.
39 H. Yang, R. Yan, H. Chen, D. H. Lee and C. Zheng, *Fuel*, 2007, **86**, 1781–1788.